

Research paper

Operation and performance of a low temperature organic Rankine cycle



Zheng Miao, Jinliang Xu^{*}, Xufei Yang, Jinghuang Zou

The Beijing Key Laboratory of Multiphase Flow and Heat Transfer for Low Grade Energy Utilization, North China Electric Power University, Beijing 102206, PR China

HIGHLIGHTS

- An organic Rankine cycle system with R123 as working fluid was tested.
- The ORC system was controlled by two independent parameters.
- The operation characteristic at hot oil temperature of 140 and 160 °C was discussed.
- Shaft powers of 2.35 kW and 3.25 kW were reached at 140 and 160 °C, respectively.
- The measured system performances were lower than the enthalpy determined ones.

ARTICLE INFO

Article history:

Received 25 September 2014

Accepted 19 October 2014

Available online 27 October 2014

Keywords:

Organic Rankine cycle

Scroll expander

Shaft torque

Shaft power

Thermal efficiency

ABSTRACT

The test and analysis of an Organic Rankine Cycle (ORC) with R123 as the working fluid were presented in this paper. A scroll expander was integrated in the system to generate work. The expander was connected with an AC dynamometer unit, which was used to control and measure the expander shaft torque and rotating speed. The conductive oil simulated the low grade heat source. Operation characteristics were compared between the heat source temperatures of 140 °C and 160 °C. The experiments were conducted by adjusting two independent parameters: the pumping frequency of the R123 pump and the shaft torque of the expander. The former parameter was directly related to the R123 mass flow rate and the later to the external load. The optimum system performance can be determined by these two parameters. The maximum measured shaft power and thermal efficiency were 2.35 kW and 6.39% at the heat source temperature of 140 °C, but they were 3.25 kW and 5.12% at the heat source temperature of 160 °C. This study identified that the measured shaft power was about 15–20% lower than the enthalpy determined values, and the pumping power of the organic fluid was 2–4 times higher than the enthalpy determined values. The enthalpy determined values were based on the local pressure and temperature sensor measurements.

© 2014 Elsevier Ltd. All rights reserved.

1. Introduction

Energy crisis and environmental protection have led to the rapidly growing interest in the utilization of low grade heat sources, such as the rejected heat from industry, solar thermal energy and geothermal heat sources. Due to the low boiling point of the organic working fluid and its simple structure, the organic Rankine cycle (ORC) is regarded as one promising technology to convert low grade heat into work [1–3]. Several medium-to-large scale (0.1–3 MW) ORC units have been available on the market [1].

However, small-scale (one to hundreds kW) ORCs are still in the infancy stage and attract more and more attention [2] because of its significant market potential in the domestic electric generation, heat recovery from the industrial boiler, and small scale CHP or other combined energy system.

During the past two decades, the ORC has been widely investigated. Most reported studies focus on the thermodynamic analysis of the ORC. And the concerns are mainly fluid selection [3–9] and parameter optimization [2,10–14]. Several conclusions with significance were drawn, such as (i) the temperature of heat source has a strong effect on the selection of working fluids and the temperature drop in the evaporator cannot be neglected [4–6]; (ii) the isentropic and dry fluids rather than wet fluids are preferred in ORCs and the thermal efficiencies for various working fluids are a

^{*} Corresponding author. Tel./fax: +86 10 61772613.

E-mail address: xjl@ncepu.edu.cn (J. Xu).

weak function of the critical temperatures [4,15]; (iii) heat transfer process in the evaporator contributes to the most irreversible loss in the whole system and the pinch temperature is a sensitive parameter to the system thermal efficiency [10,11,16]. R123 and R245fa are recommended by several groups for ORC in the recovery of low grade heat, especially at the heat source temperature of about 380–430 K [3,6,15].

Several experimental studies are also reported in recent years. The temperature of heat sources in these experimental studies was below 420 K, and R123 and R245fa were the most adopted working fluids. Most research group used scroll expander [1,17–24] in their test rig while a few used special designed expander [25–27], such as axial flow turbine or other kinds of expander [28,29]. The output power of these expanders varied from several hundred watts to several kilowatts. Bracco et al. [1] demonstrated and constructed a domestic-scale ORC prototype to recover the low grade heat. R245fa was used as the working fluid. A hermetic scroll expander was tested and the electric efficiency of about 8% was obtained while the expander inlet temperature was controlled in the range of 120–150 °C. Lemort et al. [19–21] integrated an open-drive oil-free scroll expander in an ORC and performed a series of test and modeling. While using R123 as the working fluid, the maximum overall isentropic effectiveness of 68% was achieved. And it was found that the heat loss, internal leakage and mechanical induced exergy destructions mainly accounted for the weakened expander performance. The group of Yamamoto et al. [25] is one of the earlier groups that experimentally studied the ORC. They designed a micro-turbine and integrated it into the ORC system. And R123 was suggested as a good candidate for ORC working fluids. Li et al. [26] investigated the influence of mass flow rate on the efficiency of a regenerative ORC based on a single stage axial flow turbine. Under the heat source temperature of 130 °C, the output power of 6 kW and the thermal efficiency of 7.98% were achieved. Li et al. [27,30,31] investigated a kW-scale ORC using R123 as the working fluid. The turbine was also specially designed and had a rotating speed up to 60,000 rpm. They obtained the maximum turbine power of 1 kW, the isentropic efficiency of 0.65 and the thermal efficiency of 6.8% under the temperature drop of 70 K between the turbine inlet and condenser outlet. Minea [32] analyzed a number of experimental results obtained with a 50kWe ORC based on a twin screw expander and using HFC-245fa as working fluid. The performance of this prototype was good. At heat source temperature ranging between 85 °C and 116 °C, the net heat-to-electricity conversion efficiency varied from 6.62% to 7.57%.

Although several experimental investigations have been performed, the small scale ORC is still in the infancy stage. More efforts and resources are needed to investigate the fundamental characteristics of the operation and control of small scale ORC prototype. For example, in the literature mentioned above, few works [1,19,32] measured the real output electricity or mechanical power while most other studies just calculated it based on the enthalpy differences across expander. In our former work [33], it was proved that the calculated output power derived significantly from the measured one. And the similar situation could be found in the pump. Commonly, the expander output power was overestimated while the pump consumed power was underestimated.

In the present work, we tested an ORC prototype using a 4 kW-scale scroll expander. R123 was adopted as the working fluid. An AC dynamometer controlled the expander and measured the expander performance. We focused on the steady-state operation characteristic and output performance of the ORC system. Effects of the R123 mass flow rate and the expander shaft torque on the key operating parameters, such as pressures and temperatures at expander inlet and outlet, and the system output performance, like rotating speed, shaft power and thermal efficiency, were analyzed.

Operation characteristics under heat source temperatures of 140 °C and 160 °C were compared.

2. The ORC system design and thermodynamics

Fig. 1(a) shows the design chart of the ORC flow loops in this study. This system consists of five coupled subunits: the conductive oil circuit (red lines), R123 circuit (brown lines), cooling water circuit (blue lines), lubricant oil circuit (green lines) (in web version) and AC dynamometer unit. The conductive oil was used to simulate the low grade heat source and a cooling tower is installed outdoor to cool down the cooling water flowing through the condenser. The thermodynamics of the ORC system is the same as that of the traditional steam Rankine cycle. The high pressure liquid R123 from the pump was heated into vapor in the evaporator. The heating power received by R123 is:

$$Q = m(h_{\text{eva,out}} - h_{\text{eva,in}}) \quad (1)$$

where m is the R123 mass flow rate, and $h_{\text{eva,out}}$ and $h_{\text{eva,in}}$ are R123 enthalpies at the evaporator outlet and inlet, respectively. These two enthalpies are determined by the pressures and temperatures at the evaporator outlet and inlet, respectively.

Then, the high pressure and high temperature R123 vapor expands in the expander to generate work. Fig. 1(b) shows the T-s diagram of the present ORC prototype. Points 1 and 2 can be determined by the tested temperatures and pressures at expander inlet and outlet. And the traditionally calculated shaft power of the expander in literature is given as:

$$W_{t,\text{cal}} = m(h_{t,\text{in}} - h_{t,\text{out}}) \quad (2)$$

where $h_{t,\text{in}}$ and $h_{t,\text{out}}$ are the enthalpies at the expander inlet (point 1) and outlet (point 2).

The expansion process is usually not an isentropic process, and the isentropic efficiency of the expander is commonly specified as

$$\eta_{t,s} = \frac{h_{t,\text{in}} - h_{t,\text{out}}}{h_{t,\text{in}} - h_{t,s,\text{out}}} \quad (3)$$

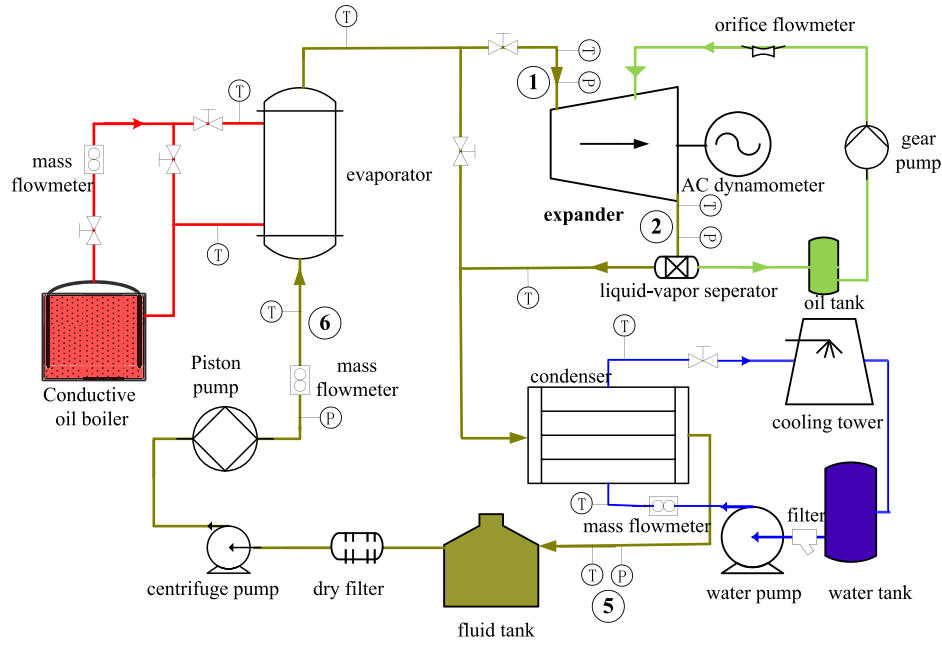
where $h_{t,s,\text{out}}$ was the outlet enthalpy through the ideal isentropic expansion process (point 2s), which could be deduced from the expander inlet entropy and expander outlet pressure.

Process 1r–2r in the T-s diagram (blue line) represents the real expansion process in the expander chamber. It is noted that, the expansion process is much complicate and, due to the limit of the testing technique, it is hard to capture the thermodynamic parameters in the expander chamber. The most common method is to locate temperature and pressure sensors at the inlet and outlet tubes of the expander. And this leads to the above mentioned derivation of the tested expansion process (1–2) from the real one (1r–2r), as the tested temperatures and pressures cannot truly reflect the losses, such as the pressure drop from the tube to the chamber, the over-expansion or under-expansion, the internal leakage and so on. Thus, in the present ORC prototype, the AC dynamometer was adopted to measure the real output power of the expander. This will be introduced in Section 3.1.

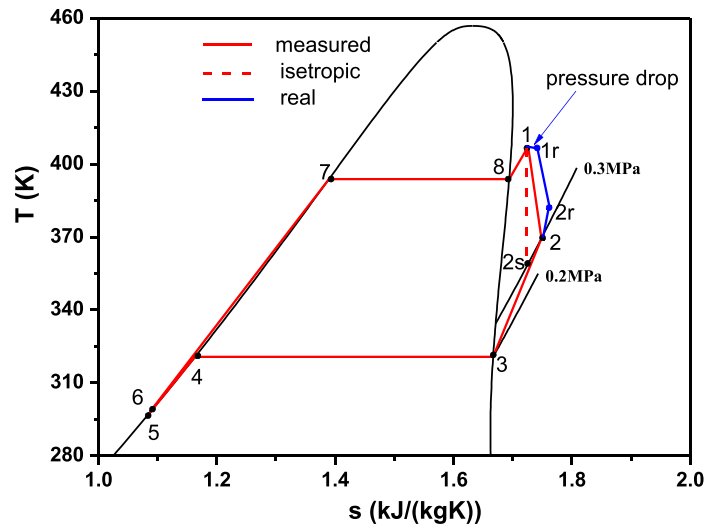
The low pressure R123 vapor exhausted from the expander is cooled down into liquid in the condenser, and cycled by the pump. The calculated power consumed by the pump is

$$W_{p,\text{cal}} = m(h_{p,\text{out}} - h_{p,\text{in}}) \quad (4)$$

where $h_{p,\text{out}}$ and $h_{p,\text{in}}$ are the fluid enthalpies at the pump outlet (point 6) and inlet (point 5), respectively. Thus, the calculated “net”



(a)



(b)

Fig. 1. Schematic representation and T-s diagram of the present ORC system.

output work and the thermal efficiency of the ORC system are as follows:

$$W_{cal} = W_{t,cal} - W_{p,cal} \quad (5)$$

$$\eta_{cal} = \frac{W_{cal}}{Q} = \frac{W_{t,cal} - W_{p,cal}}{Q} \quad (6)$$

The subscript ‘cal’ in Eqs. (2)–(6) represents that the variable is not directly measured but calculated based on the measured pressures and temperatures at various locations. In the present study, the expander output work and the power consumed by the pump were also directly measured and compare with the calculated ones. Details will be introduced in the next section.

3. The test rig description and operating procedure

3.1. The test rig description

According to the design in Fig. 1(a), the ORC prototype was constructed, which is shown in Fig. 2(a). The detailed information about this system is given as follows.

The conductive oil was heated by an electric heater with the capacity of 100 kW, which can automatically adjust the heating power to maintain the required outlet temperature with an uncertainty of 1 °C. The maximum oil temperature can reach 250 °C.

The cooling water loop was thermally coupled with the R123 circuit through the condenser. The closed spray cooling tower was installed outdoor to dissipate the extra heat of the ORC system to the air. The capacity of the cooling tower was about 73 kW at the water flow rate of 5000 kg/h and the temperature drop of 5 °C.

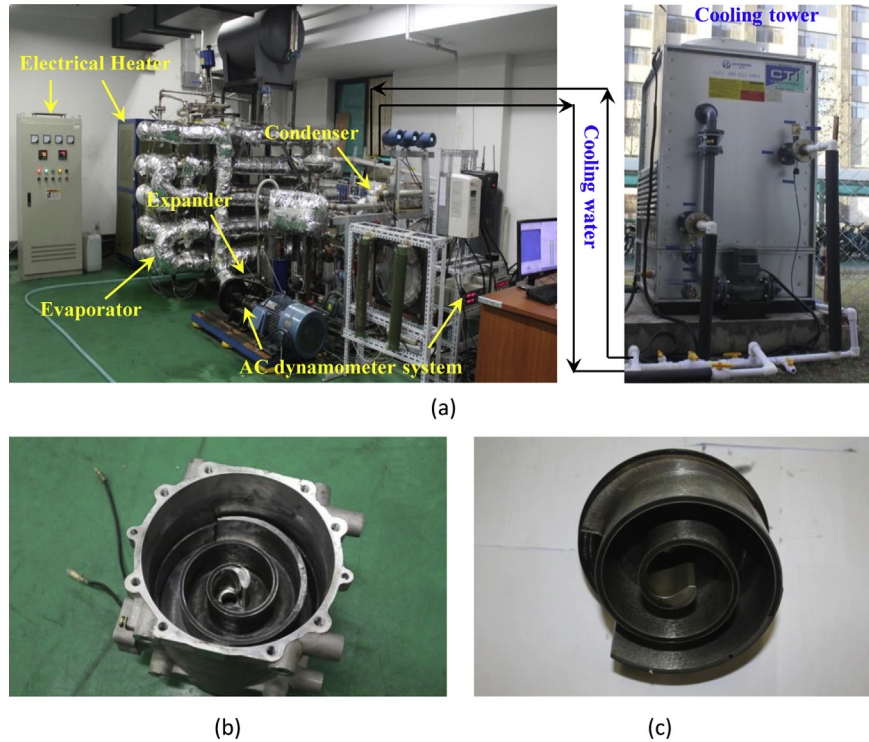


Fig. 2. The photos of (a) the experimental setup, (b) the fixed scroll and (c) the rotating scroll.

The lubricant was needed to insure the smooth operation of the expander. It was circulated by a gear pump and mixed with the R123 vapor at the expander inlet. After the expansion, it was separated from the R123 vapor by an efficient vapor-oil separator.

A tube-in-tube heat exchanger with the heat transfer area of 5.5 m^2 was used as the evaporator and a plate heat exchanger with 6.1 m^2 as the condenser. The R123 was circulated by the piston pump, which was controlled by a frequency converter. The frequency of 50 Hz corresponds to the volume flow rate of about 2000 l/h. A dry filter is located between the pump and the liquid tank to eliminate the negative effects caused by the humidity and impurity. And a centrifuge pump was installed after the dry filter to prevent the cavitation of the piston pump caused by the low boiling point and heat capacity of R123. This pump was also controlled by a frequency converter. Fig. 2(b) and (c) give the photos of fixed and rotating scrolls of the scroll expander used in the present ORC system. Due to the lack of kW-scale expander in the market, this expander was modified from a scroll compressor originally used in the bus air conditioning system. Table 1 gives the detailed geometrical parameters of the scroll expander. And the maximum shaft power of the expander was estimated about 4 kW.

In order to identify the difference between the calculated parameters in Eqs. (2)–(6) and the tested ones, an AC dynamometer unit was adopted in this work to dynamically measure the rotating speed and shaft torque of the expander. The unit consisted of a

frequency converter, an AC motor, a rotating speed sensor, a monitor, a software and transmission facilities. During the test, the shaft torque of the AC motor was set by the software and the frequency converter to be a specific percentage of the maximum value (78.5 Nm herein). Detailed information of the AC dynamometer can be found in our former work [33]. Based on the measured rotating speed and shaft torque, the output power of the expander is

$$W_{t,me} = N_t \times T_t / 9.55 \quad (7)$$

where N_t and T_t present the rotating speed and the shaft torque of the expander.

The power consumed by the R123 pump and the centrifuge pump can be obtained from the frequency converter. In such a way, the measured output power and thermal efficiency were

$$W_{me} = W_{t,me} - W_{p,me} \quad (8)$$

$$\eta_{me} = \frac{W_{t,me} - W_{p,me}}{Q} \quad (9)$$

Table 1
Geometrical parameters of the scroll expander.

Geometry parameters	
Scroll turns	2.25
Height of the scroll profile	50 mm
Thickness of the scroll profile	4.8 mm
Pitch of the scroll profile	26.5 mm
Radius of the expander	170 mm
Length of the expander	281 mm
Designed volume flow rate	211 ml/r

Table 2
Parameter measurements and uncertainties.

Parameters	Sensors	Range	Accuracy
Temperature	K-type thermocouple	−200–1300 °C	±0.5 °C
Pressure	Rosemount 3051 CG	0–1 MPa	±0.1% F.S
Pressure difference	Rosemount 3051 CD	0–5 MPa	±0.1% F.S
Mass flow rate	Coriolis mass flowmeter	0–100 kPa	±0.1% F.S
		800–8000 kg/h (water)	±0.2% flow rate
		0–3000 kg/h (R123)	
		300–3000 kg/h (oil)	
Rotating speed	JN338 rotational sensor	0–100 Nm	0.5% F.S
Shaft torque	JN338 rotational sensor	0–6000 rpm	1.0 rpm

where the subscript “me” stands for the measured value.

In the present ORC system, the measured parameters include the temperature, pressure, mass flow rate of the conductive oil, cooling water and R123 in each corresponding subsystem as well as the rotating speed and shaft torque of the expander. The location of sensors in the ORC system can be found in Fig. 1(a). And the detailed information of sensors is given in Table 2.

As several parameters in the equations mentioned above are calculated based on the measured temperatures and pressures, an error analysis was carried out based on the commonly used expression:

$$\Delta Y = \sqrt{\sum_i \left(\frac{\partial Y}{\partial X_i}\right)^2 \Delta X_i^2} \quad (10)$$

$$e_Y = \frac{\Delta Y}{Y} \quad (11)$$

where ΔY and e_Y are the uncertainty and relative uncertainty of variable Y . X_i represents the independent variable in equations. The error analysis of the key cycling parameters is given in Table 3. It is noted that the enthalpies of R123 at various state of the cycle were obtained from the software REFPROP of NIST. The state equation of R123 and the calculation process in the software are complicated. For simplification, the uncertainty of enthalpy, Δh , is estimated through the expression $\Delta h = \sqrt{\Delta h_T^2 + \Delta h_P^2}$. And, Δh_T and Δh_P are directly calculated by REFPROP from ΔT and ΔP .

3.2. The testing procedure

The closed R123 loop was initially vacuumized to remove the non-condensable gas. Then, it was charged by a certain amount of R123. From the thermodynamic point of view, the ORC system could be operated by specifying the R123 mass flow rate, temperatures and pressures. However, these parameters were not independent with each other in the closed loop during the operation. In contrast, from the control point of view, the operation of the ORC system could be specified by two accessible and independent parameters: the R123 mass flow rate and the external load of the expander, such as the shaft torque or the rotating speed. In the present ORC system, both the R123 mass flow rate and the shaft torque (or rotating speed) could be easily adjusted through the frequency converters.

In this work, two cases were carried out based on the temperature of conductive oil at the evaporator inlet, 140 °C in case 1 and 160 °C in case 2. Table 4 shows the main operating parameters. In each case, the conductive oil was controlled at a constant mass flow rate and temperature before entering the ORC evaporator. The mass flow rate of cooling water was also kept constant while the temperature at the condenser inlet varied in a narrow range due to the

Table 3
Error analysis of the key cycling parameters.

Parameter	Related variables	Average relative uncertainty
Enthalpy, h	T, P	0.5% (vapor) 0.3% (liquid)
Heat transfer rate, Q	m, h	1%
Calculated shaft power, $W_{t,cal}$	m, h	2.3%
Calculated power consumed by pump, $W_{p,cal}$	m, h	30.9%
Calculated net power output, W_{cal}	$W_{t,cal}, W_{p,cal}$	3.3%
Calculated thermal efficiency, η_{cal}	W_{cal}, Q	3.5%
Measured shaft power, $W_{t,me}$	N, T_t	0.5%
Measured thermal efficiency, η_{me}	$W_{t,me}, Q$	1.1%

changed environment temperature and condenser load. During the test, a pumping frequency of R123 pump was first set according to the temperature of conductive oil. Then the shaft torque of the expander was increased from 10% of the maximum torque load to the value at which the degree of overheat at expander inlet was too small or the shaft power of the expander exhibited a significant decrease. After that, we moved to a bigger pumping frequency and repeat the process of adjusting the expander shaft torque. When the pumping frequency reached a certain value under which the degree of overheat was too small even at the low shaft torque, the case was finished.

4. Results and discussion

4.1. Effect of the pumping frequency and shaft torque on key operation parameters

Fig. 3 shows the variation of R123 mass flow rate at different shaft torques of the expander. “ T_h ” and “PF” in the figure mean “temperature of the conductive oil” and “pumping frequency of the R123 pump”. Due to the characteristic of the piston pump, R123 mass flow rate was quite stable at every pumping frequency. The change of the shaft torque had quite limited effect on it. And an increase in PF by 1 Hz led to the increase in R123 mass flow rate by about 70 kg/h. The stability of R123 mass flow rate was beneficial to the control and smooth operation of the ORC system. At the heat source temperature of 140 °C, the proper PF was 5–8 Hz, corresponding to the R123 mass flow rate of about 350–570 kg/h. When the heat source temperature increased to 160 °C, more heat could be provided. Thus, the available PF changes to 10–13 Hz, corresponding to the R123 mass flow rate of about 660–900 kg/h.

Fig. 4 shows the vapor pressure, temperature and degrees of superheat at the expander inlet. In Fig. 4(a), for every PF, the increase in shaft torque led to the increase in vapor pressure as the stable operation of the expander need a higher vapor pressure in the chamber to balance the increased resistance on the shaft. The increase of vapor pressure also means the decrease in the volume flow rate, so as to the decrease in the expander rotating speed. For every specified shaft torque, the vapor pressure increased with the PF (representing the R123 mass flow rate). This resulted from the combine effects of the R123 volume flow rate and the irreversible losses, such as the mechanical friction, suction pressure drop and so on. As the PFs at the oil temperature of 160 °C were higher than those at 140 °C, the inlet vapor pressures were also higher. The

Table 4
Major operating parameters in this study.

Operating parameters	
Case 1: tested on Nov. 5, 2014	
Air temperature	4–16 °C
Temperature of the conductive oil	140 °C
Mass flow rate of the conductive oil	2000–2029 kg/h
Temperature of the cooling water	15.7–21.3 °C
Mass flow rate of the cooling water	2756–2763 kg/h
shaft torque	10%–70% of the maximum value
R123 pumping frequency	5.0–8.0 Hz
Case 2: tested on Nov. 4, 2014	
Air temperature	3–17 °C
Temperature of the conductive oil	160 °C
Mass flow rate of the conductive oil	2015–2034 kg/h
Temperature of the cooling water	22.1–24.7 °C
Mass flow rate of the cooling water	2769–2780 kg/h
Shaft torque	10%–90% of the maximum value
R123 pumping frequency	10.0–13.0 Hz

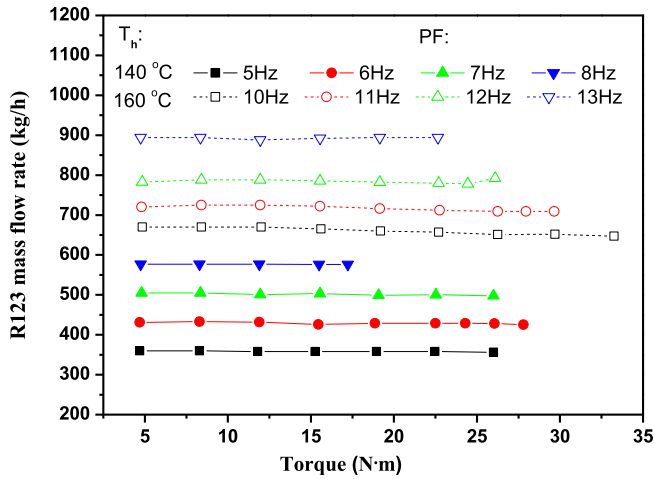


Fig. 3. Variation of R123 mass flow rates with different shaft torques.

largest vapor pressure at oil temperature of 160 °C was about 1.5 MPa while 1.2 MPa at 140 °C.

In Fig. 4(b), the variation of vapor temperature was very sensitive to the shaft torque. However, the profiles exhibited different trend for different PF. At the most PFs (6, 8 Hz and 10–11 Hz), the vapor temperature monotonically decreased with the shaft torque. This phenomenon agrees well with the heat transfer mechanism in the evaporator. The higher vapor pressure at higher shaft torque led to the enlargement of the preheating area and the shrinkage of the evaporation area. As the two-phase heat transfer coefficient is much larger than the single-phase one, the total heat flux of the evaporator became smaller. When the R123 temperature at the evaporator inlet was relatively stable, the decrease in heat flux resulted in the decrease in the vapor temperature at the expander inlet. And this process also made the vapor superheat decrease sharply, seen in Fig. 4(c). The trends of temperature profiles at PF of 5, 7, 12 and 13 Hz in Fig. 4(b) were different from those at other PFs. At 5 Hz, the R123 mass flow rate was too small, so the area of evaporator was sufficient. Under this condition, the vapor temperature was determined by the temperature difference at the outlet of the evaporator. Thus, at every shaft torque, the variation of the vapor temperature was very limited. At 7, 12 and 13 Hz, the “V” type temperature profiles were seen. Taking temperature profile at 13 Hz as an example, the reason why the vapor temperature decreased with shaft torque from 4.8 to 15.6 Nm was the same as the above mentioned heat transfer mechanism. And at shaft torque of 15.6 Nm, the vapor superheat approached 0, seen in Fig. 4(c). Then, with the further increase in shaft torque, R123 at the expander inlet went into the two-phase state, which meant the temperature herein was the saturated temperature. Thus, the higher vapor pressure at higher shaft torque led to the continued increase in R123 temperature and a “V” type temperature profile appeared.

Variations of vapor pressure, temperature and degrees of superheat at the expander outlet are shown in Fig. 5. Generally speaking, all the three variables, including vapor pressure, temperature and superheats at expander outlet decreased with the shaft torque. In Fig. 5(a), it can be seen that vapor pressure gradually decreased with the shaft torque. And the decent range was quite limited. This was because the lower heat flux in the evaporator at higher shaft torque also reduced the heat transfer load of the condenser. Thus, the vapor pressure in the condenser decreased with the shaft torque. Besides, for a specified shaft torque, it can be

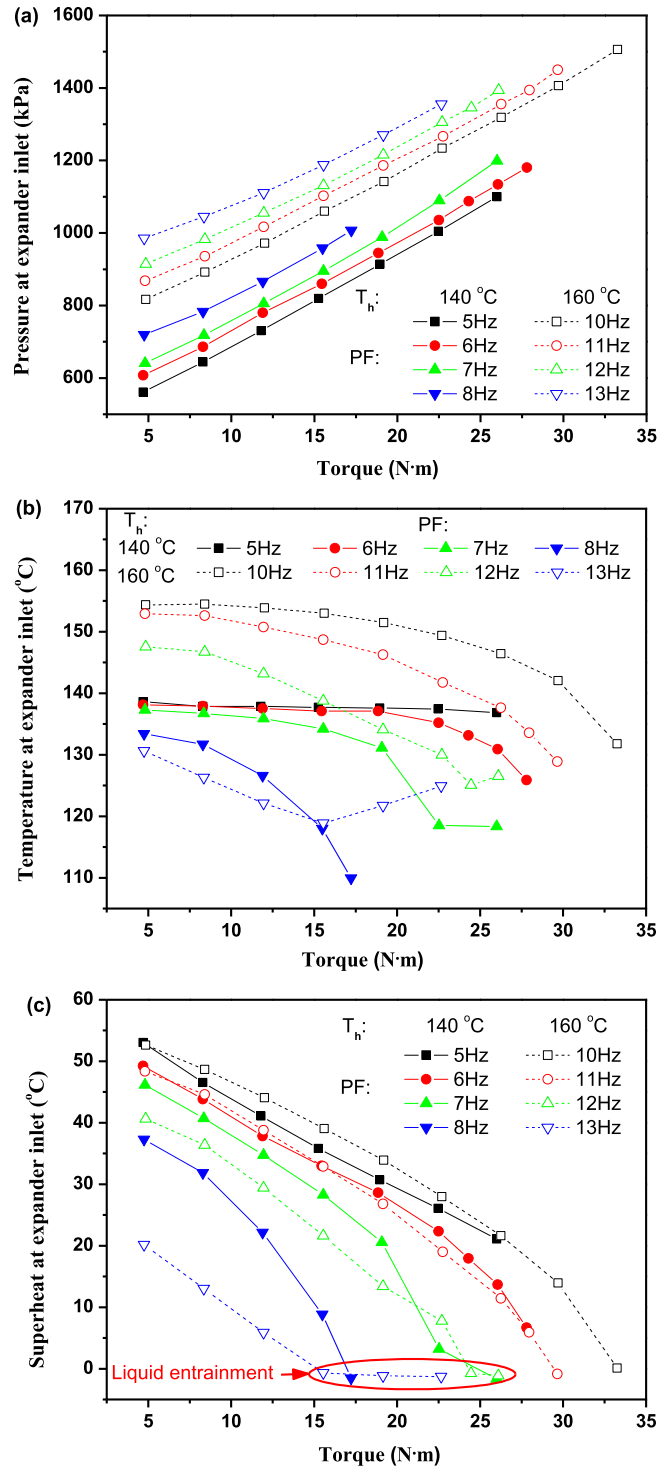


Fig. 4. Variation of vapor (a) pressures, (b) temperatures and (c) superheats at the expander inlet with different shaft torques.

observed that the vapor pressure increased with the PF as the higher R123 mass flow rate led to higher heat transfer load of the condenser. Due to the decrease of vapor temperature at the expander inlet (seen in Fig. 4(b)), it can be seen in Fig. 5(b) that the vapor temperature at the expander outlet became smaller with the increase in shaft torque. Additionally, the superheats of vapor at expander outlet also decreased with shaft torque, seen in Fig. 5(c). At the same time, in Fig. 5(b) and (c), it is obviously that the outlet

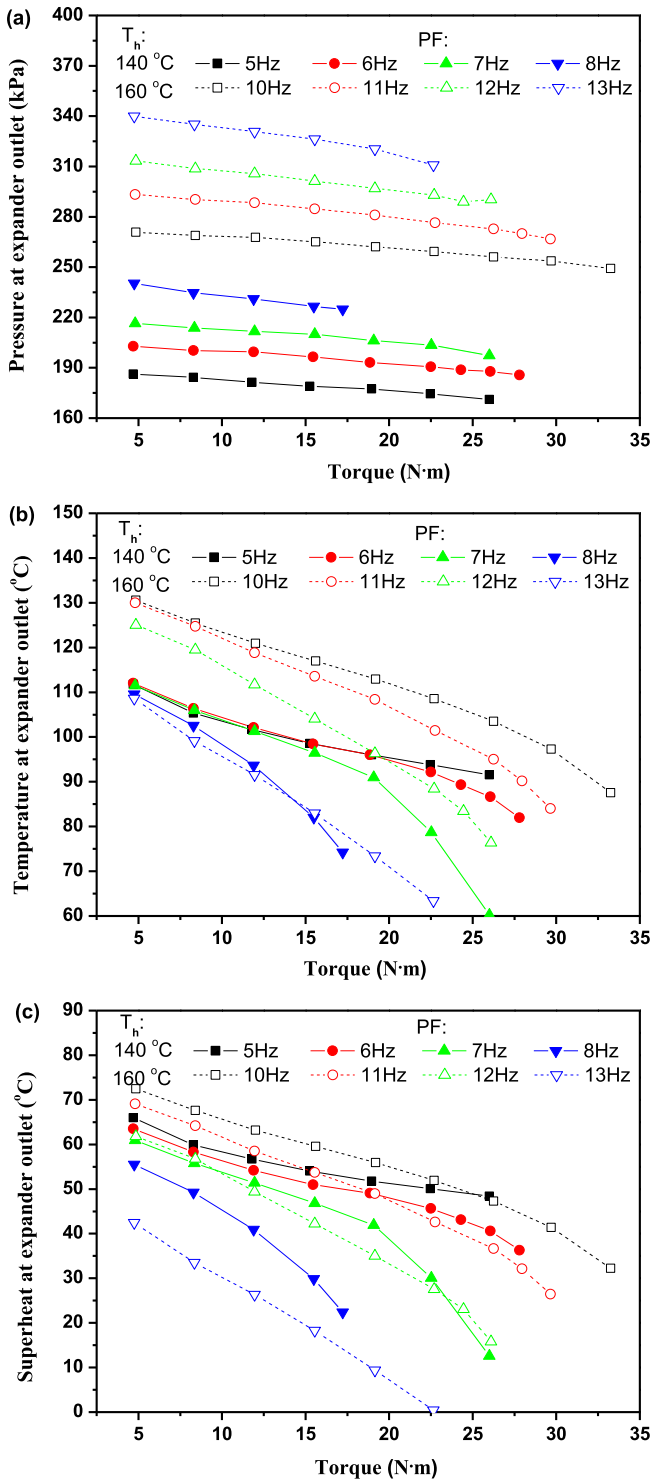


Fig. 5. Variation of vapor (a) pressures, (b) temperatures and (c) superheats at the expander outlet with different shaft torques.

vapor temperature was high, and it will be a good choice to recover this part of heat by the regenerator, such as an internal heat exchanger (IHE).

Fig. 6 shows the variation of vapor pressure, temperature and degrees of subcooling at the condenser outlet. The concern of the condensing process in the present test was whether it could provide relative stable temperature and pressure for the pump or the evaporator, and this was important for the control of the ORC

system. From Fig. 6(a) and (b), it is seen that, under a specified oil temperature, the variations of vapor pressure with both shaft torque and PF were small, limited in 15 kPa. The temperature variation with shaft torque was smaller than 1.5 K and with PF was smaller than 4 K. A closed cooling tower was used in this ORC system as a heat sink and installed outdoor. The cooling process in the cooling tower was very sensitive to the air temperature and humidity. Although the variation of environmental parameters during the

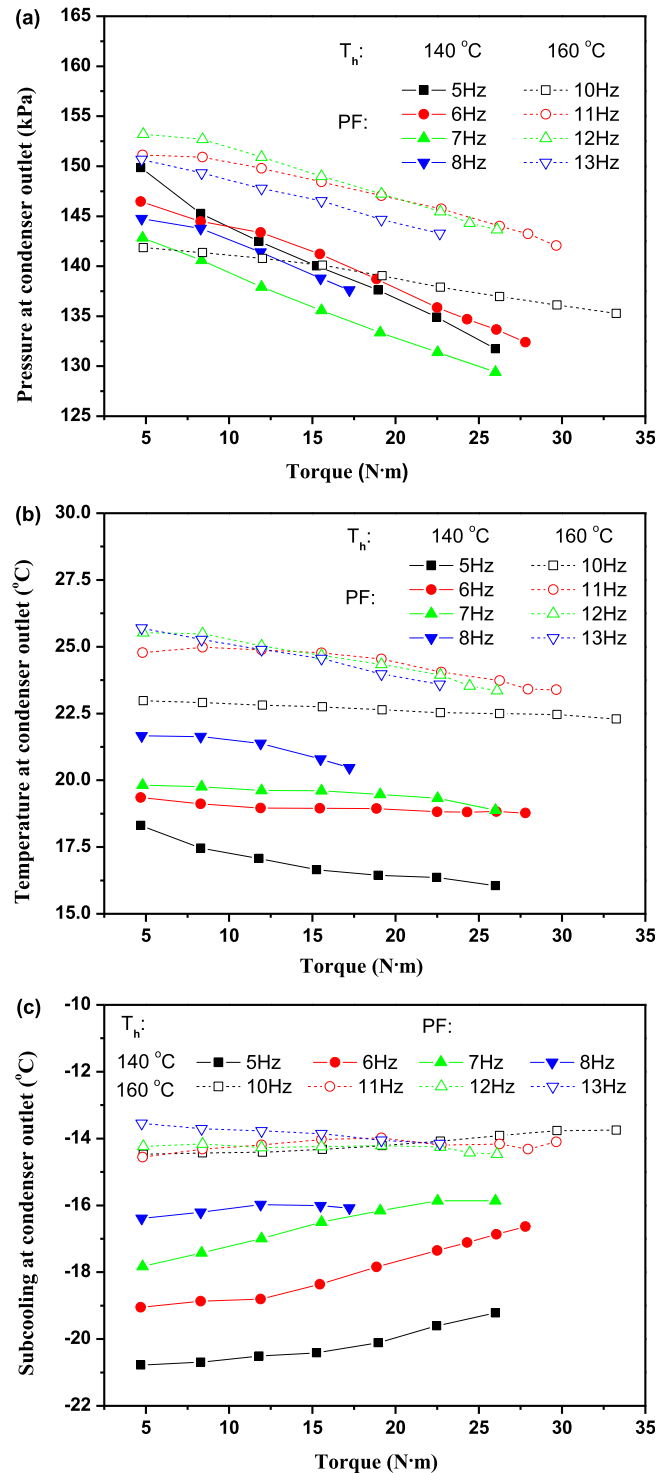


Fig. 6. Variation of vapor (a) pressures, (b) temperatures and (c) subcoolings at the condenser outlet with different shaft torques.

operation period would affect the condensing process, results in Fig. 6(a) and (b) reflects that the area of condenser was sufficient and the performance of the condensing process was good. In Fig. 6(c), the degrees of subcooling for all tested points were large, varying from -14 K to -21 K. The large degree of subcooling meant the waste of cooling source. However, for the stable working of the piston pump, a certain degrees of subcooling are required to avoid the cavitation of the pump. For the present ORC prototype, the current degrees of subcooling were not enough for the suction of the pump, so a centrifuge pump was installed between the piston pump and the fluid tank to pressurize the working fluid at the inlet of the piston pump.

4.2. Effect of the pumping frequency and shaft torque on expander performance

The pressure ratio and temperature drop through the expander were calculated based on the tested results and summarized in Fig. 7. As the pressure sensors were installed on the tubes connecting with expander inlet and outlet, the pressure ratio in Fig. 7(a) was the so called “external pressure ratio”. A bigger pressure ratio meant a higher driving force to the expander. For a given PF, the pressure ratio became higher with the increase in the shaft torque because of the step increase in the vapor pressure at the expander inlet with the shaft torque (seen in Fig. 4(a)). In

contrast, for a given shaft torque, the pressure ratio became lower with the increase in the PF due to the higher outlet vapor pressure at the higher PF. When the shaft torque was low, the effect of PF on the pressure ratio was weak. Take shaft torque at 4.8 Nm and oil temperature of 160 °C for example, the pressure ratios at all PFs were around 2.9–3.0. And, with the increase in the shaft torque, the influence of PF became significant. At the shaft torque of 19.15 Nm, the pressure ratio varied from 2.97 to 4.36. In the present test, the highest pressure ratio is about 6.5, shown in Fig. 7(a). For the adopted scroll expander, it worked in the condition of under-expansion.

In Fig. 7(b), generally speaking, the temperature drop between the inlet and outlet of the expander increased with shaft torque because the enlarged pressure drop optimized the operation of the expander. And it was also seen that temperature drop at PFs of 7, 12 and 13 Hz deviated significantly from the original trend and jumped to a very high level when the shaft torque was large. This phenomenon can be explained by the results in Fig. 4(c). The degrees of superheat at the expander inlet with large shaft torque for these three PFs were too small (around 0 °C). Thus, liquid entrainment at the expander inlet happened and led to the flash evaporation of R123 droplets in the expander chambers. The latent heat of the phase change made the vapor temperature decrease significantly. At the same time, the too small degrees of R123 superheat also meant the increase of R123 temperature at the expander inlet with the increase in shaft torque, which had been mentioned above. As a result, the temperature drop became very large.

Fig. 8 shows the variation of the rotating speed of the expander with different shaft torques. Clearly, the rotating speed decreased with the shaft torque. And for a specified shaft torque, the larger PF led to the higher rotating speed as long as R123 at the expander inlet was at vapor phase. When liquid entrainment occurred, the rotating speed decreased rapidly and deviated from the original trend. Besides, when justifying the PF from 5 Hz to 6 Hz and then to 7 Hz, the rotating speed increased fast. However, when the PF was higher than 8 Hz, the increase of PF had very limited effect on rotating speed.

Based on the tested temperatures and pressures at expander inlet and outlet, the isentropic efficiencies were calculated and shown in Fig. 9. It is noted that the enthalpy and entropy of R123 at expander inlet could not be determined by the tested temperature and pressure when liquid entrainment occurred as the mass fraction of liquid in vapor phase was unknown. Consequently, the

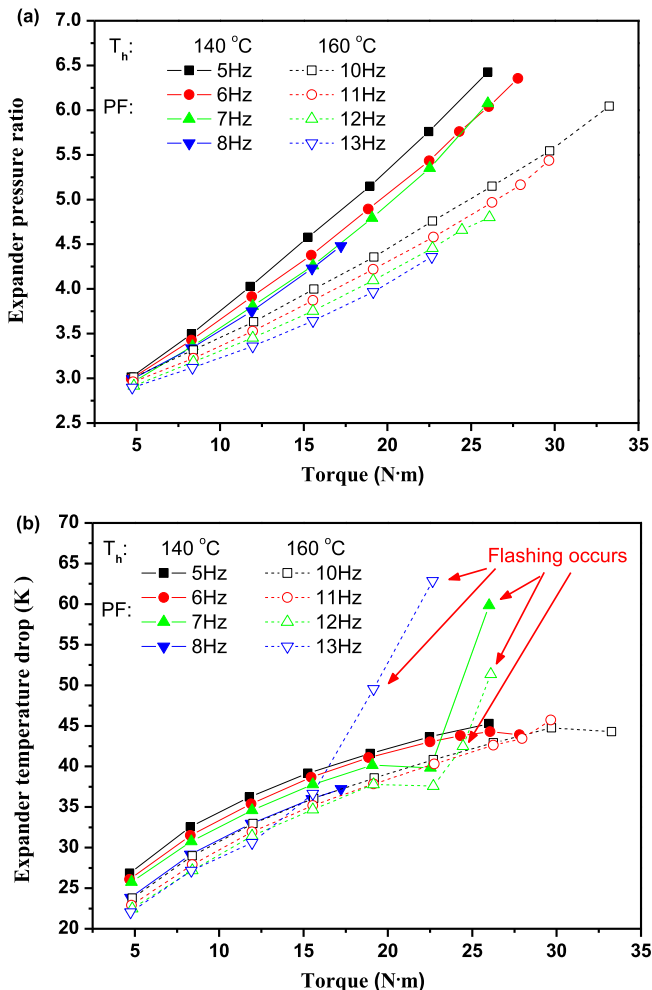


Fig. 7. Variation of the (a) pressure ratio and (b) temperature drop of the expander with different shaft torques.

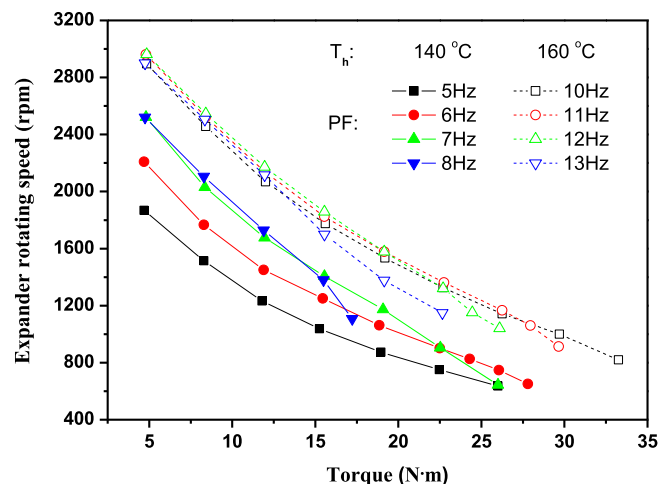


Fig. 8. Variation of the rotating speed of the expander with different shaft torques.

isentropic efficiencies under those situations were not obtained and given in Fig. 9. It can be seen that, for a given PF, the expander isentropic efficiency first increased with the shaft torque, reached the peak, and then decreased with the further increase in the shaft torque. The mechanism of how the sensitive factors, such as heat release to the environment, pressure loss in suction and exhaust, mechanical friction and internal leakage affect the isentropic efficiency was very complicated. And it was hard to explain the trends just based on the experimental results. Lemort et al. [19] modeled the scroll expander and obtained the trend of isentropic efficiency versus the pressure ratio. And our results in Fig. 9 agree well with their results. Besides, the increase in PF led the decrease in expander isentropic efficiency at a specified shaft torque, seen in Fig. 9.

4.3. Deviation of the system performance and the calculated one

In the above sections, we have mentioned the deviation of tested expander shaft power and pump consumed power from the calculated ones due to the location where temperature and pressure sensors were installed. In our former work [33], we compared the tested performance with the calculated one under two operating mode and at the heat source temperature of 150 °C. In the present work, the tested results and calculated ones in more working points are compared and shown in Figs. 10–12 to summarize the fundamental principles. Comparison of the tested shaft powers with the calculated ones is shown in Fig. 10. On one hand, the calculated shaft powers were much higher than the tested ones. At oil temperature of 140 °C, the highest calculated shaft power was 2940 W while the tested one was 2350 W, approximately 20% lower. And the data for oil temperature of 160 °C are 3820 W, 3245 W and 15% lower. On the other hand, the profiles of calculated shaft power exhibited similar trends with tested ones. The shaft power was the product of the shaft torque and rotating speed. So either too smaller shaft torque or too lower rotating speed would lead to the decrease in the shaft power. As a result, at a specified PF in Fig. 10, the shaft power first increased with shaft torque, reached the highest value and then went down. Besides, when the PF was low, the increase in the PF could improve the shaft power. However, when the PF was high, the further increase in the PF could make the expander encounter the liquid entrainment prematurely, which would bring down the shaft power. In Fig. 10, it was seen that, for the present ORC system, the proper PFs are 7 Hz for 140 °C and 11 Hz for 160 °C.

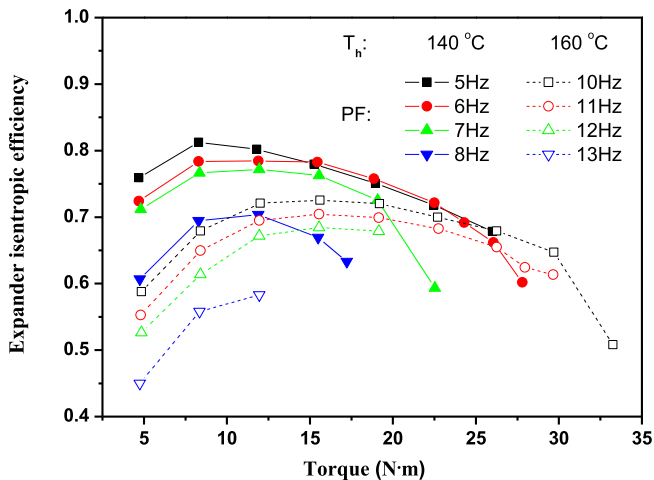


Fig. 9. Variation of the isentropic efficiency of the expander with different shaft torques.

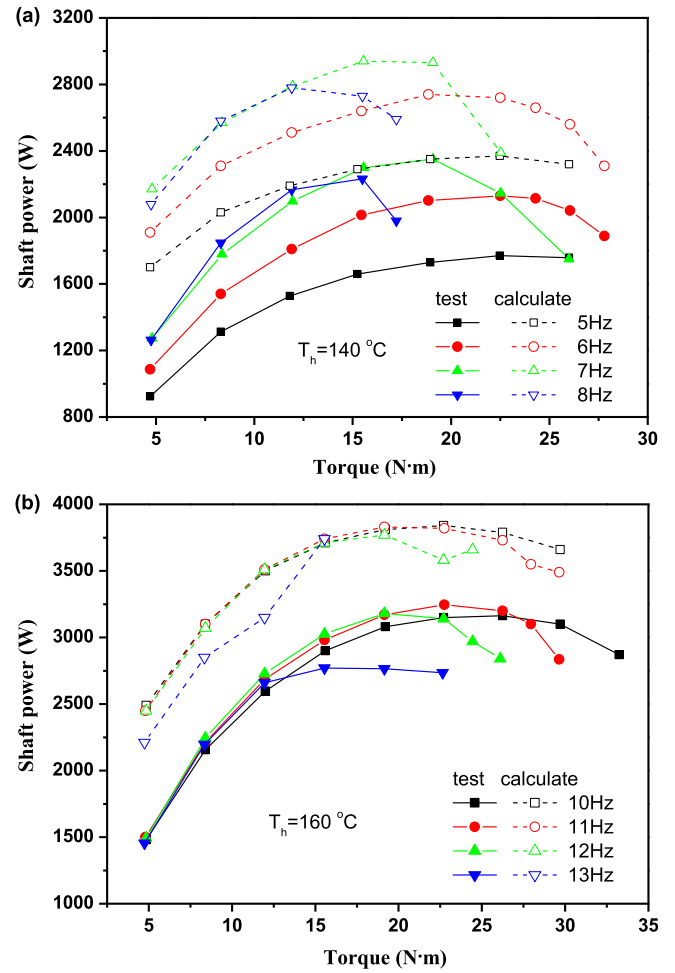


Fig. 10. Comparison of the tested shaft powers of the expander and the calculated ones, (a) temperature of heat source 140 °C, (b) temperature of heat source 160 °C.

Fig. 11 shows the comparison of the tested pump consumed powers and the calculated ones. In ORC literature, the power consumed by pump was always neglected. However, in Fig. 11, it was apparently that the pump consumed a big part of the power produced from expander. Corresponding to the highest shaft power in Fig. 10, the pump consumed power was about 11.5% of the total power output at 140 °C, and 29.9% at 160 °C, seen in Fig. 11(a) and (b). This was due to the low efficiency of pump in the real ORC system. The real consumed powers were about 2 or 4 times higher than the calculated ones from Eq. (4). Improvement of pump efficiency was required for the commercialization of the small ORC system.

The comparison of the tested system thermal efficiencies and the calculated ones is given in Fig. 12. Because of the overestimate of the calculated shaft power and underestimate of the calculated pump consumed power, the calculated system thermal efficiencies in Fig. 12 were much higher than the tested ones. At oil temperature of 140 °C, the highest calculated thermal efficiency was 9.51% while the tested one was 6.39%. With the increase of oil temperature from 140 °C to 160 °C, both the calculated and the tested thermal efficiencies became smaller due to the rapid increase of heat flux in the evaporator. The highest ones for 160 °C are 7.05% and 5.12%, respectively. The big difference between the calculated and tested ORC performance indicates that the calculated performance based on the measured temperatures and pressures can mislead the design of the ORC system to a certain extent. So the basic tested

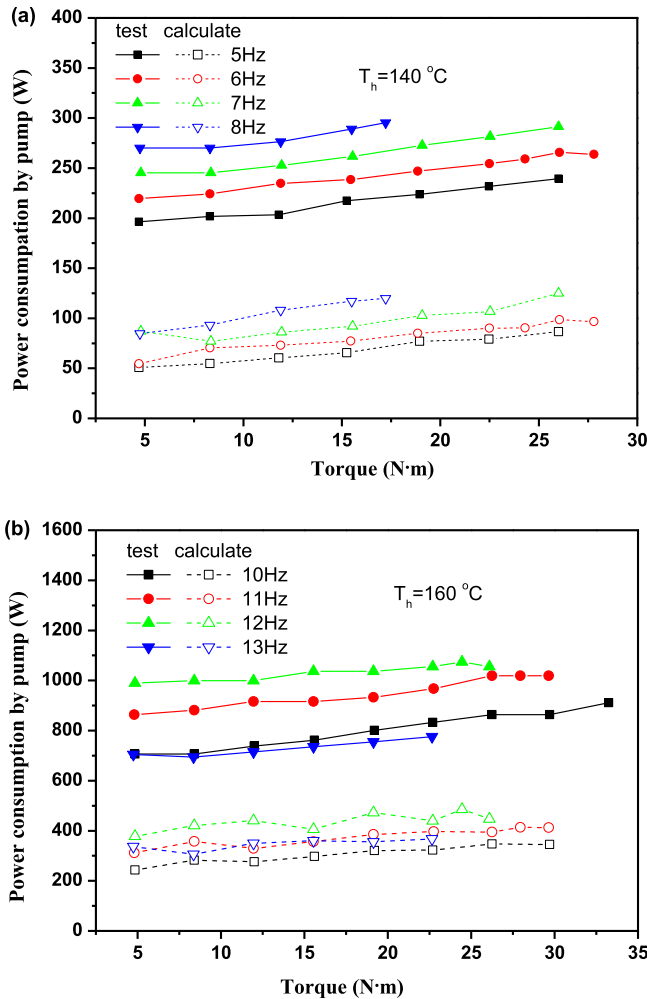


Fig. 11. Comparison of the tested power consumptions by the pump and the calculated ones, (a) temperature of heat source 140 °C, (b) temperature of heat source 160 °C.

data and comprehensive numerical model of the ORC system are important for the commercialization of the ORC technique.

5. Conclusions

Focusing on the exploration of kW-scale ORC system, this study presented the test and analysis of the operation characteristics and performance of an ORC prototype with R123 as the working fluid. A scroll expander was adopted and connected with an AC dynamometer unit to record the shaft power and rotating speed in real time. Operation characteristics under heat source temperatures of 140 °C and 160 °C were compared. The main findings are summarized below:

- (1) The ORC system can be controlled by two independent parameters: the R123 mass flow rate and the external load. The optimum system performance can be determined by these two parameters. The maximum measured shaft power under 140 °C were 2.35 kW while 3.25 W under 160 °C.
- (2) Although the increase in temperature of the conductive oil led to the increase in expander shaft power, the thermal efficiency became smaller due to the sharp increase in heat flux in the evaporator. The highest thermal efficiencies under 140 °C and 160 °C were 6.39% and 5.12%, respectively.

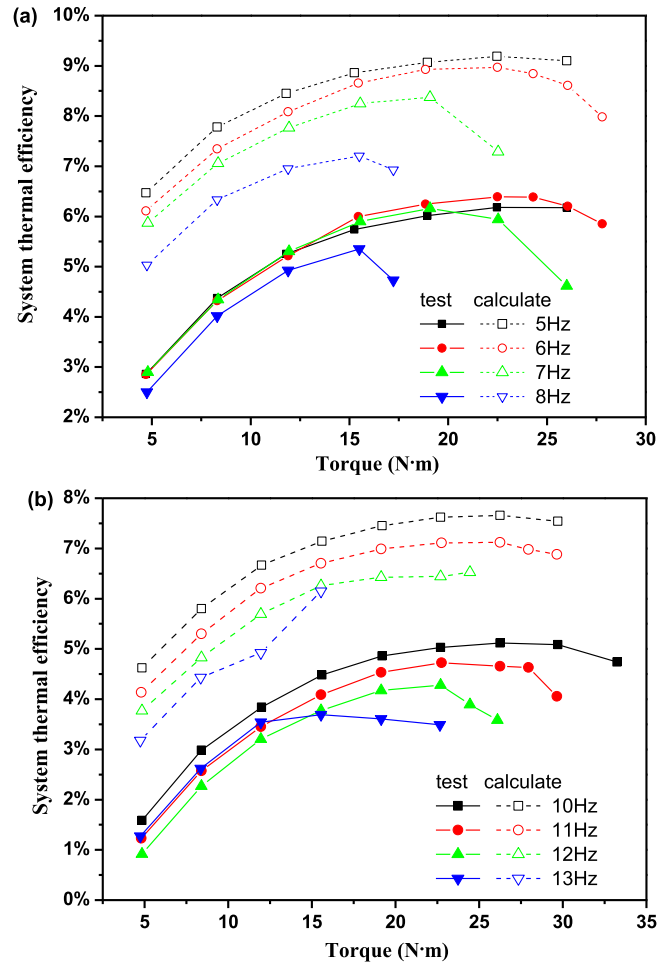


Fig. 12. Comparison of the tested system thermal efficiencies and the calculated ones, (a) temperature of heat source 140 °C, (b) temperature of heat source 160 °C.

- (3) As it is hard to install sensors in the expander chamber, the tested temperature and pressure in the tube close to the expander inlet and outlet resulted in the deviation of the enthalpy determined system performance from the tested ones. The measured shaft powers were 15–20% lower than the calculated ones and the pump consumed powers were 2–4 times higher than the calculated ones.

Acknowledgements

This work was supported by the National Natural Science Foundation of China (51306048), the International cooperation project of NSFC (51210011) and the 973 project (2011CB710703).

Nomenclature

- List of symbols
R expansion ratio
T shaft torque (Nm)

- Subscripts
evp evaporator
p pump
s isentropic process
t turbine, expander

References

- [1] R. Bracco, S. Clemente, D. Micheli, M. Reini, Experimental tests and modelization of a domestic-scale ORC (Organic Rankine Cycle), *Energy* 58 (2013) 107–116.
- [2] S. Clemente, D. Micheli, M. Reini, R. Tacconi, Energy efficiency analysis of organic Rankine cycles with scroll expanders for cogenerative applications, *Appl. Energy* 97 (2012) 792–801.
- [3] T.-C. Hung, Waste heat recovery of organic Rankine cycle using dry fluids, *Energy Convers. Manage.* 42 (2001) 539–553.
- [4] B.T. Liu, K.H. Chien, C.C. Wang, Effect of working fluids on organic Rankine cycle for waste heat recovery, *Energy* 29 (2004) 1207–1217.
- [5] W.C. Andersen, T.J. Bruno, Rapid screening of fluids for chemical stability in organic Rankine cycle applications, *Ind. Eng. Chem. Res.* 44 (2005) 5560–5566.
- [6] P.J. Mago, L.M. Chamra, C. Somayaji, Performance analysis of different working fluids for use in organic Rankine cycles, *Proc. Inst. Mech. Eng. Part A J. Power Energy* 221 (2007) 255–264.
- [7] B. Saleh, G. Koglbauer, M. Wendland, J. Fischer, Working fluids for low-temperature organic Rankine cycles, *Energy* 32 (2007) 1210–1221.
- [8] B.F. Tchanche, G. Papadakis, G. Lambrinos, A. Frangoudakis, Fluid selection for a low-temperature solar organic Rankine cycle, *Appl. Therm. Eng.* 29 (2009) 2468–2476.
- [9] T.C. Tung, S.K. Wang, C.H. Kuo, B.S. Pei, K.F. Tsai, A study of organic working fluids for use in organic Rankine cycles, *Energy* 35 (2010) 1403–1411.
- [10] C. He, C. Liu, H. Gao, H. Xie, Y.R. Li, S.Y. Wu, J.L. Xu, The optimal evaporation temperature and working fluids for subcritical organic Rankine cycle, *Energy* 38 (2012) 136–143.
- [11] Y.R. Li, J.N. Wang, M.T. Du, Influence of coupled pinch point temperature difference and evaporation temperature on performance of organic Rankine cycle, *Energy* 42 (2012) 503–509.
- [12] C. Liu, C. He, H. Gao, H. Xie, Y.R. Li, S.Y. Wu, J.L. Xu, The environmental impact of organic Rankine cycle for waste heat recovery through life-cycle assessment, *Energy* 56 (2013) 144–154.
- [13] D. Wei, X. Lu, Z. Lu, J. Gu, Dynamic modeling and simulation of an Organic Rankine Cycle (ORC) system for waste heat recovery, *Appl. Therm. Eng.* 28 (2008) 1216–1224.
- [14] J. Xu, C. Liu, Effect of the critical temperature of organic fluids on supercritical pressure organic Rankine cycles, *Energy* 63 (2013) 109–122.
- [15] H. Chen, D.Y. Goswami, E.K. Stefanakos, A review of thermodynamic cycles and working fluids for the conversion of low-grade heat, *Renewable Sustainable Energy Rev.* 14 (2010) 3059–3067.
- [16] Q. Chen, J. Xu, H. Chen, A new design method for organic Rankine cycles with constraint of inlet and outlet heat carrier fluid temperatures coupling with the heat source, *Appl. Energy* 98 (2012) 562–573.
- [17] T. Li, J. Zhu, W. Fu, K. Hu, Experimental comparison of R245fa and R245fa/R601a for organic Rankine cycle using scroll expander, *Int. J. Energy Res.* (2014) (published online).
- [18] J.A. Mathias, J.R. Johnston, J. Cao, D.K. Priedeman, R.N. Christensen, Experimental testing of gerotor and scroll expander used in, and energetic and exergetic modeling of, an organic Rankine cycle, *J. Energy Resour. Technol.* 131 (2009) 012201.
- [19] V. Lemort, S. Quoilin, C. Cuevas, J. Lebrun, Testing and modeling a scroll expander integrated into an organic Rankine cycle, *Appl. Therm. Eng.* 29 (2009) 3094–3102.
- [20] S. Quoilin, V. Lemort, J. Lebrun, Experimental study and modeling of an organic Rankine cycle using scroll expander, *Appl. Energy* 87 (2010) 1260–1268.
- [21] S. Declaye, S. Quoilin, L. Guillaume, V. Lemort, Experimental study on an open-drive scroll expander integrated into an ORC (Organic Rankine Cycle) system with R245fa as working fluid, *Energy* 55 (2013) 173–183.
- [22] D. Manolakos, G. Papadakis, S. Kyritsis, K. Bouzianas, Experimental evaluation of an autonomous low-temperature solar Rankine cycle system for reverse osmosis desalination, *Desalination* 203 (2007) 366–374.
- [23] D. Manolakos, G. Kosmadakis, S. Kyritsis, G. Papadakis, Identification of behaviour and evaluation of performance of small scale low-temperature organic Rankine cycle system coupled with a RO desalination unit, *Energy* 34 (2009) 767–774.
- [24] D. Manolakos, G. Kosmadakis, S. Kyritsis, G. Papadakis, On site experimental evaluation of a low-temperature solar organic Rankine cycle system for RO desalination, *Sol. Energy* 83 (2009) 646–656.
- [25] T. Yamamoto, T. Furuhashi, N. Arai, K. Mori, Design and testing of the organic Rankine cycle, *Energy* 26 (2001) 239–251.
- [26] M.Q. Li, J.F. Wang, W.F. He, L. Gao, B. Wang, S.L. Ma, Y.P. Dai, Construction and preliminary test of a low-temperature regenerative Organic Rankine Cycle (ORC) using R123, *Renewable Energy* 57 (2013) 216–222.
- [27] G. Pei, J. Li, Y. Li, D. Wang, J. Ji, Construction and dynamic test of a small-scale organic Rankine cycle, *Energy* 36 (2011) 3215–3223.
- [28] N. Zheng, L. Zhao, X.D. Wang, Y.T. Tan, Experimental verification of a rolling-piston expander that applied for low-temperature organic Rankine cycle, *Appl. Energy* 112 (2013) 1265–1274.
- [29] X.D. Wang, L. Zhao, J.L. Wang, W.Z. Zhang, X.Z. Zhao, W. Wu, Performance evaluation of a low-temperature solar Rankine cycle system utilizing R245fa, *Sol. Energy* 84 (2010) 353–364.
- [30] J. Li, G. Pei, Y. Li, D. Wang, J. Ji, Energetic and exergetic investigation of an organic Rankine cycle at different heat source temperatures, *Energy* 38 (2012) 85–95.
- [31] J. Li, G. Pei, Y. Li, D. Wang, J. Ji, Examination of the expander leaving loss in variable organic Rankine cycle operation, *Energy Convers. Manage.* 65 (2013) 66–74.
- [32] V. Minea, Power generation with ORC machines using low-grade waste heat or renewable energy, *Appl. Therm. Eng.* 69 (2014) 143–154.
- [33] Z. Miao, X. Yang, J. Xu, J. Zou, Development and dynamic characteristics of an organic Rankine cycle, *Chin. Sci. Bull.* 59 (2014) 4367–4380.